



Highly efficient deep-blue light-emitting material based on V-Shaped donor-acceptor triphenylamine-phenanthro[9,10-d]imidazole molecule

Yue Yu^a, Ruiyang Zhao^{b,c}, Haichao Liu^{c,**}, Shitong Zhang^c, Changjiang Zhou^c, Yu Gao^c, Weijun Li^{a,c,*}, Bing Yang^c

^a State Key Laboratory Breeding Base of Green Chemistry Synthesis Technology, College of Chemical Engineering, Zhejiang University of Technology, Hangzhou, 310014, PR China

^b College of Chemical Engineering, Qingdao University of Science and Technology, Qingdao, 266042, PR China

^c State Key Lab of Supramolecular Structure and Materials, Jilin University, 2699 Qianjin Avenue, Changchun, 130012, PR China

ARTICLE INFO

Keywords:

phenanthro[9,10-d]imidazole
Deep blue materials
HLCT
OLEDs

ABSTRACT

Based on novel phenanthro[9,10-d]imidazole (PI) chromophore, three deep-blue luminescent donor-acceptor molecules with different molecular configurations at the triphenylamine (TPA) core were designed and synthesized, the linear TPA-1PI, the V-shaped TPA-2PI and the star-shaped TPA-3PI. All three molecules displayed the hybridized local and charge-transfer (HLCT) excited state character, and highly efficient deep blue emissions were observed in their solution state, but only those of linear TPA-1PI and V-shaped TPA-2PI molecule were maintained in the solid state. Meanwhile, the V-shaped TPA-2PI and star-shaped TPA-3PI showed the much better thermal properties. Thus the molecular configurations of HLCT materials significantly influence their solid-state, and the V-shaped TPA-2PI molecule was highlighted because of its both deep-blue emission and good thermal stability. A double-layer device by using TPA-2PI as the emitter showed a highly efficient deep-blue electroluminescence with a very good CIE coordinate of (0.14, 0.08) and high current efficiency of 2.7 cd A⁻¹, which suggest that it might be a promising candidate for emission-layer materials for high-performance deep-blue OLEDs.

1. Introduction

Since the discovery of the multilayer thin-film structures in organic light-emitting diodes (OLEDs) by Tang et al. [1–8], through the huge efforts of scientists, OLEDs have been broadly applied commodities such as in displays and, to some extent, as lighting sources. Compared with red [9–11] and green [12–14] counterparts with satisfactory performance, blue organic emitters, especially the deep-blue organic emitters have attracted huge research attention as a consequence of their present day poor colour purity, unbalanced charge injection and transport due to its wide band gap. Although there were a lot of blue emitters have been reported, high-performance blue emitters [15–18] with good color quality and high electroluminescent efficiency (EL) are still urgently required to be further developed with great attention. Among them, phenanthro[9,10-d]imidazole (PI) based derivatives have shown the great potential for high-performance electroluminescent materials

based on their good color purity with narrow FWHM (full width at half maximum) [19], balanced charge carrier injection/transporting ability [20], high fluorescent efficiency [21] as well as high exciton utilization efficiency [22–24], indicating that PI should be a perfect building unit for designing deep-blue emitters.

In this work, with triphenylamine (TPA) group as the donor part, a series of newly-designed PI-based deep-blue luminescent donor-acceptor molecule TPA-1PI, TPA-2PI and TPA-3PI with linear, V-shaped and star-shaped molecular configurations respectively were developed for blue-emitted electroluminescent materials. In the film state, the V-shaped TPA-2PI could maintain its deep-blue emission with high quantum efficiency. The non-doped OLEDs based on TPA-2PI as emitter layer were fabricated, and finally a highly efficient deep blue electroluminescence was obtained with a CIE coordinate of (0.14, 0.08) and an external quantum efficiency of 2.6%. These results demonstrate that the V-shaped TPA-2PI molecule might serve as a potential candidate for

* Corresponding author. State Key Laboratory Breeding Base of Green Chemistry Synthesis Technology, College of Chemical Engineering, Zhejiang University of Technology, Hangzhou, 310014, PR China.

** Corresponding author.

E-mail addresses: hliu@jlu.edu.cn (H. Liu), liwj@zjut.edu.cn (W. Li).

<https://doi.org/10.1016/j.dyepig.2020.108511>

Received 30 December 2019; Received in revised form 30 April 2020; Accepted 30 April 2020

Available online 7 May 2020

0143-7208/© 2020 Elsevier Ltd. All rights reserved.

high-performance deep-blue emitters in OLEDs.

2. Experimental

2.1. Materials and measurement

All the reagents and solvents used for the synthesis were purchased from Aldrich or Acros companies and used as received. All reactions were performed under a dry nitrogen atmosphere. The ^1H NMR spectra were recorded on AVANCZ 500 spectrometers at 298 K by utilizing deuterated chloroform (CDCl_3) or dimethyl sulphoxide (DMSO) as solvent and tetramethylsilane (TMS) as standard. The compounds were characterized by Flash EA 1112, CHNS-O elemental analysis instrument. The HRMS (ESI) mass spectra were recorded using a Bruker micrOTOF-Q II instrument. UV-vis absorption spectra were recorded on UV-3100 spectrophotometer. Fluorescence measurements were carried out with RF-5301PC. Thermal gravimetric analysis (TGA) was undertaken on a PerkinElmer thermal analysis system at a heating rate of $10\text{ }^\circ\text{C min}^{-1}$ and a nitrogen flow rate of 80 mL min^{-1} . The differential scanning calorimeter (DSC) analysis was determined using a NETZSCH (DSC-204) instrument at $10\text{ }^\circ\text{C min}^{-1}$ under nitrogen flushing. Cyclic voltammetry (CV) were performed with a BAS 100 W Bioanalytical Systems, using a glass carbon disk ($\Phi = 3\text{ mm}$) as working electrode, platinum wire as auxiliary electrode with porous ceramic wick, Ag/Ag^+ as reference electrode, standardized for the redox couple ferricinium/ferrocene. All solutions were purged with nitrogen stream for 10 min before measurement. The procedure was performed at room temperature and nitrogen atmosphere was maintained over the solution during measurements.

2.2. Device fabrication

The EL devices were fabricated by vacuum deposition of the materials at 10^{-6} Torr onto ITO glass with a sheet resistance of $25\text{ }\Omega\text{ square}^{-1}$. All of the organic layers were deposited at a rate of $1.0\text{ }\text{Å}^{-1}$. The cathode was deposited of LiF (1 nm) at a deposition rate of $0.1\text{ }\text{Å}^{-1}$ and then capping with Al metal (100 nm) through thermal evaporation at a rate of $4.0\text{ }\text{Å}^{-1}$. The electroluminescent (EL) spectra and Commission Internationale De L'Eclairage (CIE) coordinations of these devices were measured by a PR650 spectroscan spectrometer. The luminance-current and density-voltage characteristics were recorded simultaneously with the measurement of the EL spectra by combining the spectrometer with a Keithley model 2400 programmable voltage-current source. All measurements were carried out at room temperature under ambient conditions.

2.3. Synthesis

2.3.1. 4-(diphenylamino)benzaldehyde (M1)

Triphenylamine (5.0 g, 20.3 mmol) was dissolved in DMF (10 mL). POCl_3 (1.9 mL, 20.3 mmol) was added dropwise to the mixture at $0\text{ }^\circ\text{C}$. After mixing, the temperature was raised to room temperature, during which the color of the solution turned red. The reaction mixture was then heated to $60\text{ }^\circ\text{C}$ and stirred for an additional 2 h. The product mixture was poured into an ice-bath and neutralized with sodium bicarbonate. After filtration, the residue was dried over P_2O_5 in a vacuum drier, then purified by column chromatography using CH_2Cl_2 as the eluent. Pale yellow solid (5.4 g, 96%). MP: $120\text{ }^\circ\text{C}$. IR data (KBr): 1693, 1592, 1503, 1430, 1392, 1322, 1290, 1217, 1168, 820, 710, 650, 532 cm^{-1} . ^1H NMR (500 MHz, DMSO) δ 9.77 (s, 1H), 7.72 (d, $J = 8.7\text{ Hz}$, 2H), 7.42 (t, $J = 7.8\text{ Hz}$, 4H), 7.28–7.15 (m, 6H), 6.89 (d, $J = 8.7\text{ Hz}$, 2H). HRMS (ESI) m/z : $[\text{M} + \text{H}]^+$ calcd for $\text{C}_{19}\text{H}_{16}\text{NO}$: 274.1217, found 274.1226.

2.3.2. 4,4'-(phenylazanediyldibenzaldehyde (M2)

Triphenylamine (5.0 g, 20.3 mmol) was dissolved in DMF (10 mL).

POCl_3 (9.4 mL, 102.0 mmol) was added dropwise to the mixture at $0\text{ }^\circ\text{C}$. After mixing, the temperature was raised to room temperature, during which the color of the solution turned red. The reaction mixture was then heated to $60\text{ }^\circ\text{C}$ and stirred for an additional 2 h. The product mixture was poured into an ice-bath and neutralized with sodium bicarbonate. After filtration, the residue was dried over P_2O_5 in a vacuum drier, then purified by column chromatography using CH_2Cl_2 as the eluent. Yellow solid (6.4 g, 90%). MP: $143\text{ }^\circ\text{C}$. IR data (KBr): 1694, 1587, 1505, 1493, 1426, 1392, 1331, 1292, 1217, 1167, 1112, 822, 762, 701 cm^{-1} . ^1H NMR (500 MHz, DMSO) δ 9.88 (s, 2H), 7.84 (d, $J = 8.7\text{ Hz}$, 4H), 7.47 (t, $J = 7.9\text{ Hz}$, 2H), 7.31 (t, $J = 7.4\text{ Hz}$, 1H), 7.24–7.20 (m, 2H), 7.17 (d, $J = 8.6\text{ Hz}$, 4H). HRMS (ESI) m/z : $[\text{M} + \text{H}]^+$ calcd for $\text{C}_{20}\text{H}_{16}\text{NO}_2$: 302.1173, found 302.1176.

2.3.3. 4,4',4''-nitrotribenzaldehyde (M3)

M2 (2.4 g, 8.2 mmol) was dissolved in 8 mL DMF (8 mL). POCl_3 (10.0 mL, 100.0 mmol) was added dropwise to the mixture at $0\text{ }^\circ\text{C}$. After mixing, the temperature was raised to room temperature, during which the color of the solution turned red. The reaction mixture was then heated to $60\text{ }^\circ\text{C}$ and stirred for an additional 2 h. The product mixture was poured into an ice-bath and neutralized with sodium bicarbonate. After filtration, the residue was dried over P_2O_5 in a vacuum drier, then purified by column chromatography using CH_2Cl_2 as the eluent. Yellow solid (2.1 g, 80%). MP: $245\text{ }^\circ\text{C}$. IR data (KBr): 1694, 1589, 1504, 1434, 1392, 1322, 1275, 1217, 1168, 819, 724 cm^{-1} . ^1H NMR (500 MHz, DMSO) δ 9.94 (s, 3H), 7.91 (d, $J = 8.5\text{ Hz}$, 6H), 7.28 (d, $J = 8.5\text{ Hz}$, 6H). HRMS (ESI) m/z : $[\text{M} + \text{H}]^+$ calcd for $\text{C}_{21}\text{H}_{16}\text{NO}_3$: 330.1115, found 330.1125.

2.3.4. N,N-diphenyl-4-(1-phenyl-1H-phenanthro[9,10-d]imidazole-2-yl)aniline (TPA-1PI)

A mixture of aniline (5.0 mmol, 465 mg), phenanthrenequinone (1.0 mmol, 208.0 mg), intermediate M1 (1.0 mmol, 237.0 mg), ammonium acetate (4.0 mmol, 308.0 mg), and acetic acid (8 mL) was refluxed under nitrogen in an oil bath. After 2 h, the mixture was cooled and filtered. The solid product was washed with an acetic acid/water mixture (15 mL, 1:1) and water. And then, it was purified by chromatography using CH_2Cl_2 as eluent. white solid (483.0 mg, 90%). MP: $285\text{ }^\circ\text{C}$. IR data (KBr): 1588, 1516, 1485, 1468, 1453, 1424, 1383, 1330, 1281, 1195, 1076, 1037, 966, 840, 747, 735, 720 cm^{-1} . ^1H NMR (500 MHz, DMSO) δ 8.92 (d, $J = 7.9\text{ Hz}$, 1H), 8.87 (d, $J = 8.3\text{ Hz}$, 1H), 8.67 (d, $J = 7.9\text{ Hz}$, 1H), 7.77 (t, $J = 7.5\text{ Hz}$, 1H), 7.70–7.64 (m, 1H), 7.57–7.51 (m, 1H), 7.47 (d, $J = 8.8\text{ Hz}$, 2H), 7.39–7.29 (m, 4H), 7.11 (t, $J = 7.4\text{ Hz}$, 2H), 7.05 (t, $J = 7.7\text{ Hz}$, 4H), 6.83 (d, $J = 8.8\text{ Hz}$, 2H). HRMS (ESI) m/z : $[\text{M} + \text{H}]^+$ calcd for $\text{C}_{39}\text{H}_{28}\text{N}_3$: 538.2278, found 538.2278.

2.3.5. N-phenyl-4-(1-phenyl-1H-phenanthro[9,10-d]imidazole-2-yl)-N-(4-(1-phenyl-1H-phenanthro[9,10-d]imidazole-2-yl)phenyl)aniline (TPA-2PI)

A mixture of aniline (10.0 mmol, 930.0 mg), phenanthrenequinone (2.0 mmol, 516.0 mg), intermediate M2 (1.0 mmol, 301.0 mg), ammonium acetate (8.0 mmol, 616.0 mg), and acetic acid (8.0 mL) was refluxed under nitrogen in an oil bath. After 2 h, the mixture was cooled and filtered. The solid product was washed with an acetic acid/water mixture (15 mL, 1:1) and water. And then, it was purified by chromatography using CH_2Cl_2 as eluent. White solid (730.4 mg, 88%). MP: $362\text{ }^\circ\text{C}$. IR data (KBr): 1738, 1597, 1536, 1514, 1494, 1471, 1453, 1382, 1344, 1320, 1286, 1265, 1183, 1073, 1037, 920, 837, 754, 723 cm^{-1} . ^1H NMR (500 MHz, DMSO) δ 8.92 (d, $J = 8.3\text{ Hz}$, 2H), 8.87 (d, $J = 8.3\text{ Hz}$, 2H), 8.68 (d, $J = 7.9\text{ Hz}$, 2H), 7.81–7.65 (m, 14H), 7.57–7.52 (m, 2H), 7.51 (d, $J = 8.8\text{ Hz}$, 4H), 7.35 (dt, $J = 15.5, 8.1\text{ Hz}$, 4H), 7.17 (t, $J = 7.4\text{ Hz}$, 1H), 7.06 (t, $J = 8.7\text{ Hz}$, 4H), 6.90 (d, $J = 8.8\text{ Hz}$, 4H). HRMS (ESI) m/z : $[\text{M} + \text{H}]^+$ calcd for $\text{C}_{60}\text{H}_{40}\text{N}_5$: 830.3277, found 830.3278.

2.3.6. tris(4-(1-phenyl-1H-phenanthro[9,10-d]imidazole-2-yl)phenyl)amine (TPA-3PI)

A mixture of aniline (15.0 mmol, 1.4 g), phenanthrenequinone (3.0

mmol, 624.0 mg), intermediate M3 (1.0 mmol, 330.0 mg), ammonium acetate (12.0 mmol, 924.0 mg), and acetic acid (8 mL) was refluxed under nitrogen in an oil bath. After 2 h, the mixture was cooled and filtered. The solid product was washed with an acetic acid/water mixture (15 mL, 1:1) and water. And then, it was purified by chromatography using CH_2Cl_2 as eluent. White solid (898.0 mg, 80%). MP: 423 °C. IR data (KBr): 1911, 1693, 1594, 1495, 1470, 1379, 1320, 1291, 1218, 1162, 1107, 1038, 935, 920, 836, 754, 723, 698, 670, 615, 533 cm^{-1} . $^1\text{H NMR}$ (500 MHz, DMSO) δ 8.91 (d, $J = 8.4$ Hz, 3H), 8.86 (d, $J = 8.4$ Hz, 3H), 8.67 (d, $J = 7.9$ Hz, 3H), 7.80–7.65 (m, 21H), 7.53 (dd, $J = 14.2, 8.4$ Hz, 9H), 7.32 (t, $J = 7.7$ Hz, 3H), 7.05 (d, $J = 8.0$ Hz, 3H), 6.92 (d, $J = 8.8$ Hz, 6H). HRMS (ESI) m/z : [M + H]⁺ calcd for $\text{C}_{81}\text{H}_{52}\text{N}_7$: 1122.4279; Found: 1122.4293.

3. Results and discussion

3.1. Synthesis and characterization

The molecular structures of linear TPA-1PI, V-shaped TPA-2PI and star-shaped TPA-3PI are shown in Fig. 1, and all three new compounds were efficiently synthesized in a one-pot multicomponent reaction from low cost precursors, which is very important for its future commercial applications. The mixture of aniline, phenanthrenequinone, ammonium acetate and corresponding aromatic aldehyde were refluxed for 2 h, then cooled to room temperature and filtered. Their crude products were purified by chromatography and the yields of all target products were above 75%. The $^1\text{H NMR}$ spectra of TPA-1PI, TPA-2PI and TPA-3PI in the aromatic range are shown in Fig. 2. The doublets at 8.93, 8.87 and 8.67 ppm together with the triplets at 7.53 and 7.32 ppm correspond to the proton resonance of the 1-, 8-, 4-, 3-, 6-protons of the phenanthro [9,10-*d*]imidazole structure respectively for all the three compounds. All the peaks observed in the $^1\text{H NMR}$ spectra are consistent with their respective structures.

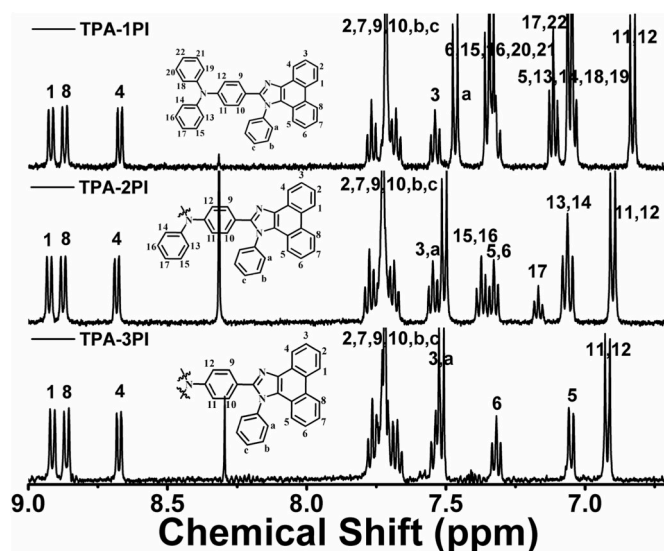


Fig. 2. $^1\text{H NMR}$ spectra of PI derivatives in the aromatic range.

3.2. UV and PL spectra

As shown in Fig. 3, in the solution state, TPA-1PI, TPA-2PI and TPA-3PI showed the absorption peaks at 360 nm, 376 nm and 378 nm, respectively. And they all exhibited the deep-blue emission with λ_{max} at 420, 424, and 426 nm, respectively. Therefore stoke's shifts of three compounds in solution were 60 nm, 48 nm and 48 nm, respectively. There was no obvious big difference between their photoluminescence (PL) spectra except for some little spectra shift. In film state, all the PL emissions from these three molecules showed red shifts but still localized in the blue spectral zone with λ_{max} at 438 nm for TPA-1PI, 458 nm for TPA-2PI, and 489 nm for TPA-3PI, respectively. Compared to those in solution state, all the three molecules showed the redshift of PL

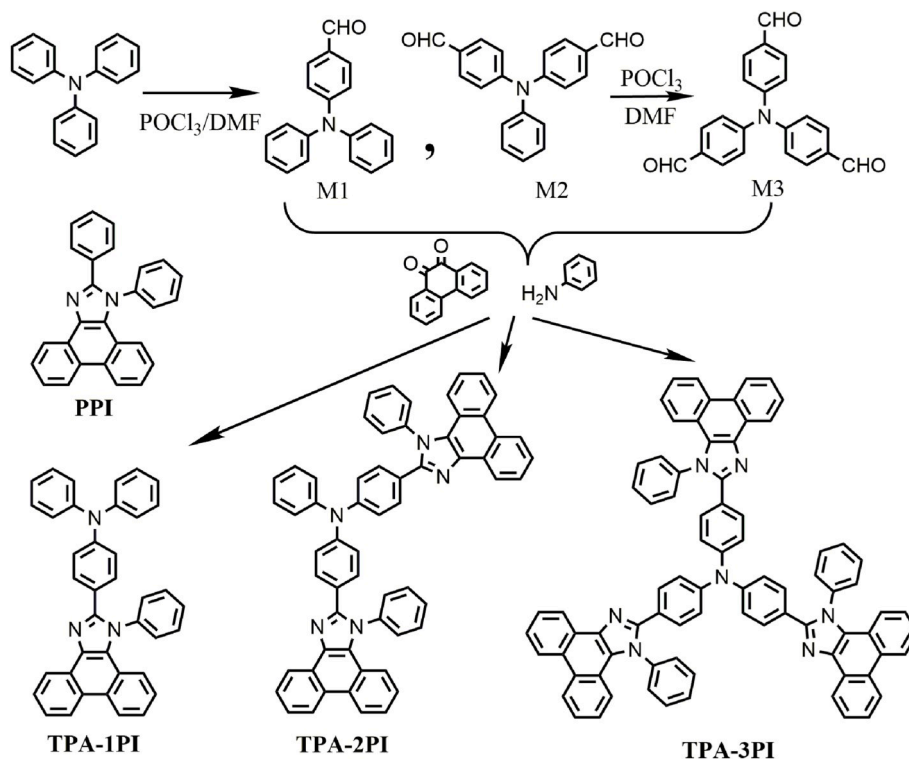


Fig. 1. The synthetic route and molecular structures of linear TPA-1PI, V-shaped TPA-2PI and star-shaped TPA-3PI.

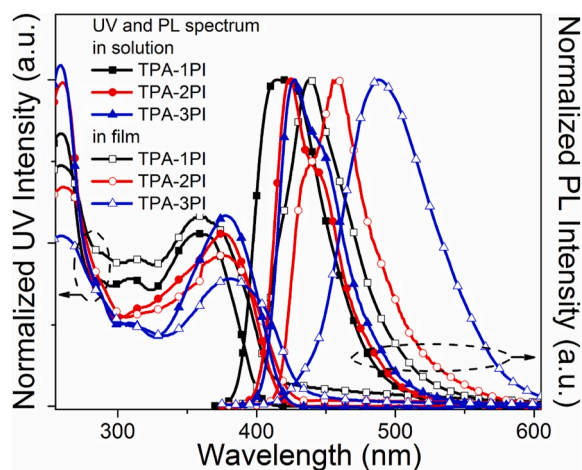


Fig. 3. The normalized UV and PL spectra of linear TPA-1PI, V-shaped TPA-2PI and star-shaped TPA-3PI in solution (10^{-5} mol L^{-1} , chloroform) and film state.

spectra in solid state. This might be ascribed to the aggregated-state intermolecular π - π stack due to the existence of large π -conjugated plane of PI unit in their molecular structure. The redshift of PL spectra in star-shaped TPA-3PI was much larger than those of linear TPA-1PI and V-shaped TPA-2PI. This indicated that their molecular configurations should induce the different aggregated-state structures, which resulted in different redshifts of PL spectra in solid state. It was obvious that the spectra of TPA-1PI and TPA-2PI belong to the deep-blue emission while

that of TPA-3PI should be attributed to the sky-blue emission. From this point, only TPA-1PI and TPA-2PI could serve as the deep-blue electro-luminescent emitters.

The fluorescence quantum yields (Φ_f) were determined to be as high as 0.65 for TPA-1PI, 0.75 for TPA-2PI and 0.85 for TPA-3PI in THF solution by using quinine sulphate in 1 M sulphuric acid as a standard, and 0.30 for TPA-1PI, 0.40 for TPA-2PI and 0.40 for TPA-3PI in the solid state by using an integrating sphere photometer. Compared to the high Φ_f values in solution state, those of TPA-1PI, TPA-2PI and TPA-3PI in film state were relatively lower. This might be ascribed to the quenching effect of intermolecular π - π stack in solid state, which were consistent with those results of redshifted PL spectra from solution to solid state.

3.3. Solvatochromic properties

Solvatochromism experiments were carried out to further study their excited state properties for the three PI-based molecules, as shown in Fig. 4. In low-polarity butyl ether, TPA-1PI, TPA-2PI and TPA-3PI exhibited split peaks emission with λ_{max} at 405 nm, 415 nm and 419 nm, respectively, which indicated that all of them possessed the LE-state characteristic. As for high-polarity acetonitrile, the fluorescence spectra of these three PI-based molecules broadened and exhibited singlet peak emission with λ_{max} at 427 nm, 439 nm and 440 nm, respectively which possessed the CT-state characteristic. Along with this process when the solvent polarity was increased gradually from low polarity to high polarity, these three PI-based molecules exhibited a similar redshift of about 20 nm (22 nm for TPA-1PI, 25 nm for TPA-2PI and 21 nm for TPA-3PI). In these molecules, they could possess the hybridized local and charge-transfer (HLCT) excited state [25–28], in which the LE state had a bigger contribution due to the smaller solvatochromic spectra shift and the obvious split peaks in most solvents. These three PI-based molecules presented a similar change in solvatochromism experiments and it indicated they possessed the similar HLCT character at the lowest excited state in which LE state had bigger contribution.

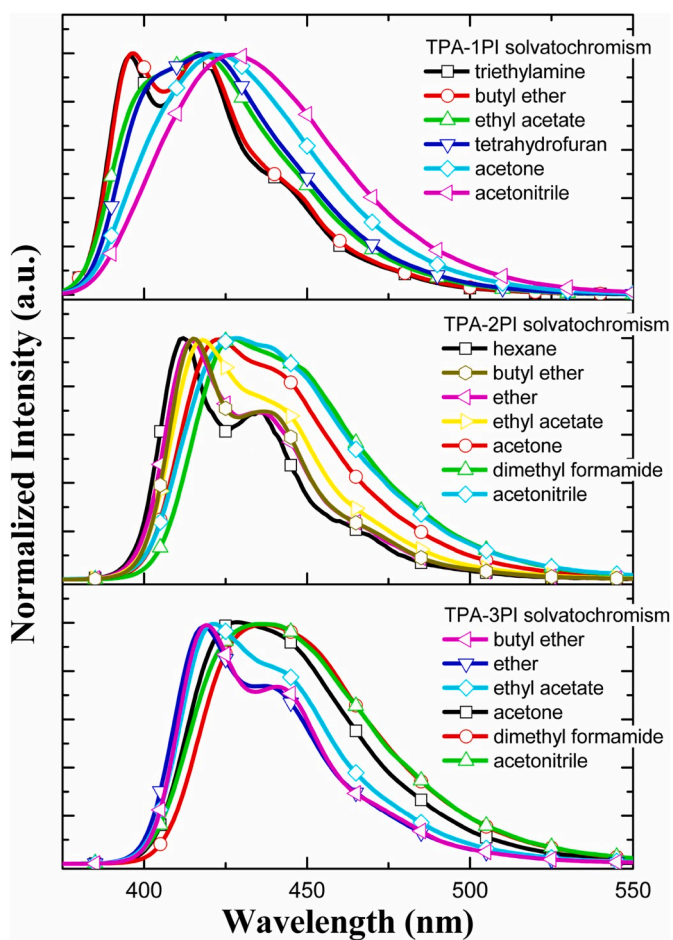


Fig. 4. PL spectra of linear TPA-1PI, V-shaped TPA-2PI and star-shaped TPA-3PI, measured in different solvents with increasing polarity.

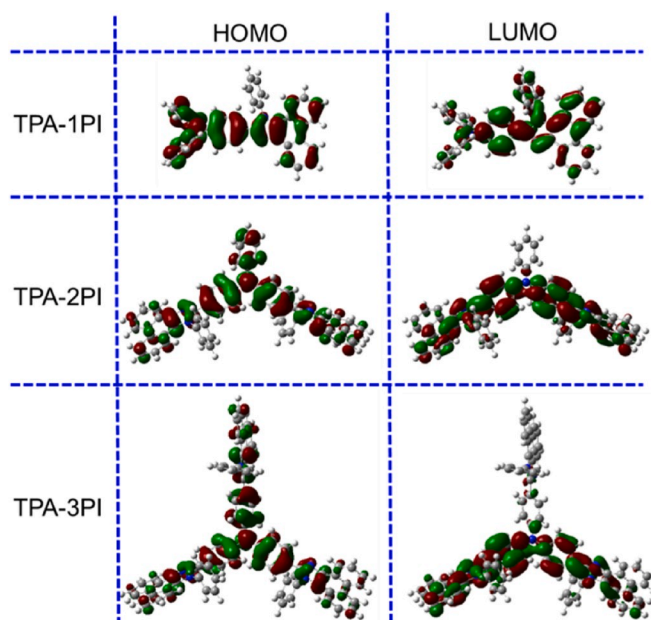


Fig. 5. The frontier molecular orbitals (HOMO and LUMO) in the ground state of linear TPA-1PI, V-shaped TPA-2PI and star-shaped TPA-3PI.

3.4. DFT calculation

Density functional theory (DFT) calculations of frontier molecular orbitals by CAM-B3LYP method were also studied to investigate the electronic transition character in the three molecules. In spite of different molecular configurations in the linear TPA-1PI, V-shaped TPA-2PI and star-shaped TPA-3PI, these three PI-based molecules possessed similar frontier molecular orbital as shown in Fig. 5, and both the highest occupied molecular orbital (HOMO) and lowest unoccupied molecular orbital (LUMO) delocalized over the whole molecule, instead of being fully separated (or localized partially). In this case, HOMO → LUMO should not be treated as a pure-CT transition, but a HLCT state with mainly LE transition. These DFT analyses further proved that the different molecular configurations of these three PI-based molecules had little effect on their single-molecule excited state properties. The different redshifts of PL spectra (in Fig. 3) from solution to solid state of these three PI-based molecules should be ascribed to different aggregated-state structures induced by their different molecular configurations.

3.5. Electrochemical properties

The electrochemical properties of TPA-1PI, TPA-2PI and TPA-3PI were characterized by cyclic voltammetry (CV) method as shown in Fig. 6. CV curves of the three molecules exhibited one reversible redox peak at the positive potential range, all of which were similar to that of TPA. The same onset oxidative potential of 0.55 V was obtained for all three molecules, giving a HOMO level of -5.18 eV for TPA-1PI, TPA-2PI and TPA-3PI by comparison to ferrocene. Compared to that of PI (HOMO level of -5.53 eV) [20], the HOMO levels of TPA-1PI, TPA-2PI and TPA-3PI were obviously higher, indicating enhanced hole injection ability, which should be ascribed to the importance of the TPA donor group with lower ionization energy^[2L]. The CV analysis also gave the LUMO levels of -2.12 , -2.16 , and -2.19 eV for TPA-1PI, TPA-2PI and TPA-3PI respectively, which were close to that of PI (LUMO level of -2.15 eV). The CV analysis of HOMO and LUMO energy levels in linear TPA-1PI, V-shaped TPA-2PI and star-shaped TPA-3PI reflected the import of TPA group into molecular structure really improved hole carrier injection ability in these three materials without influencing the injection ability of electron carrier.

3.6. Thermal properties

All three PI-based derivatives showed high thermal stabilities. As

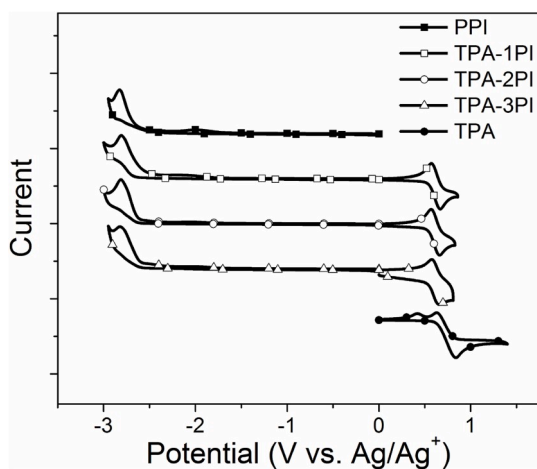


Fig. 6. The electrochemistry curves of linear TPA-1PI, V-shaped TPA-2PI and star-shaped TPA-3PI with those of PI under negative potential and TPA under positive potential as reference.

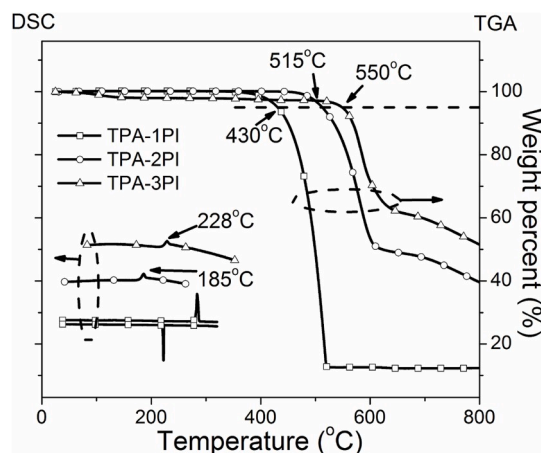


Fig. 7. The measured thermal curves of differential scanning calorimeter (DSC, left) and thermal gravimetric analyzer (TGA, right) for linear TPA-1PI, V-shaped TPA-2PI and star-shaped TPA-3PI.

shown in Fig. 7, the temperatures for 5% weight loss were estimated to be 430 °C, 515 °C and 550 °C for TPA-1PI, TPA-2PI and TPA-3PI, respectively, which were much higher than that of PI (340 °C). More importantly, TPA-2PI and TPA-3PI could form amorphous films with very high glass transition temperature (T_g) of 185 °C and 228 °C, respectively, which were distinctly higher than that of PI (62 °C). Such high T_g values implicated that they could form morphologically stable amorphous films upon thermal evaporation, which was highly important for application in OLEDs. While TPA-1PI showed the obviously

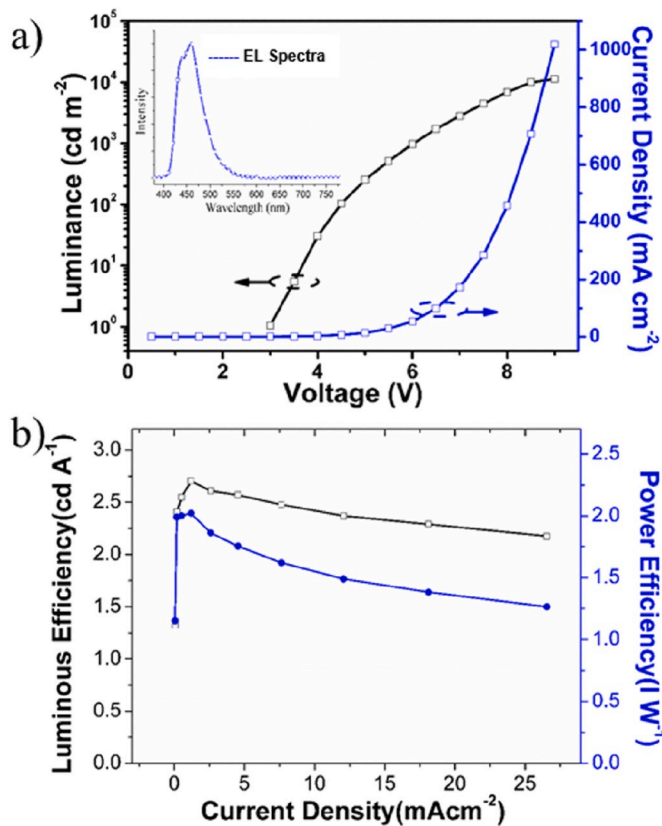


Fig. 8. a) The current density–voltage–luminance curves (inset graph was the EL spectra of the device) and b) current efficiency versus current density curves of device based on TPA-2PI.

repeated melting and crystallization peaks during the whole heating and cooling program, which indicated that TPA-1PI tended to form as crystalline state in solid. These results also demonstrated that the different molecular configurations of TPA-1PI, TPA-2PI and TPA-3PI brought the different aggregation-state structures and associated properties.

3.7. Device performance

Considering the sky-blue emission of TPA-3PI in the film state and the thermal properties of TPA-1PI, the non-doped electroluminescent devices based on TPA-2PI (deep blue emission in film and highly thermal stability) as emitters were fabricated in order to obtain the highly efficient deep blue electroluminescence which was more desirable and significant for the current organic light emitting diode applications. The device configurations of ITO/PEDOT:PSS (40 nm)/TPA-2PI (30 nm)/TPBi (50 nm)/LiF/Al was fabricated, in which TPBi was utilized as the hole-blocking and electron-transporting layer. The results in Fig. 8 showed that this device displayed a deep blue electroluminescence with λ_{\max} at 458 nm, which was consistent with the previous PL spectra of TPA-2PI in the solid state. The obtained deep blue electroluminescence of TPA-2PI based device corresponded to a CIE coordinate of (0.14, 0.08), which matched well with the blue standards (0.14, 0.08) of the National Television Standards Committee (NTSC). As for the performance, the device based on TPA-2PI as emitter also exhibited a maximum luminance of 11,309 cd m^{-2} , a maximum current efficiency of 2.7 cd A^{-1} and a maximum power efficiency of 2.0 l m W^{-1} , equivalent to an external quantum efficiency (EQE) of 2.6%. These results indicated TPA-2PI to potentially serve as a highly efficient deep blue emitter in OLEDs with excellent color purity.

4. Conclusion

In summary, with a triphenylamine (TPA) group as the donor part and phenanthro[9,10-*d*]imidazole (PI) blocks as the acceptor part, a series of newly-designed deep-blue luminescent D-A molecules TPA-1PI, TPA-2PI and TPA-3PI with linear, V-shaped and star-shaped molecular configurations respectively were developed for blue-emitting electroluminescent materials. Experimental measurement and theoretical calculation indicated that all these materials displayed HLCT character and exhibited similar photophysical properties in single molecule but different ones in solid state which was aroused by their different molecular configurations. After a systematic comparison of these three molecules, TPA-2PI can act as a high-performance emitter out of comprehensive consideration of deep-blue emission, high fluorescence efficiency and good thermal stability. The non-doped OLED based on TPA-2PI as emitter was fabricated, and a highly efficient deep-blue electroluminescence was obtained with a CIE coordinate of (0.14, 0.08) and an EQE of 2.6%. These results demonstrate that the V-shaped TPA-2PI molecule might serve as a potential candidate for high-performance deep-blue emitters in OLEDs. The device with a simple structure shows good device performance, rendering the prospect of this material in the actual applications. This work also demonstrates a strategy of chemical structure modification to improve material properties.

Declaration of competing interest

The authors declare that they have no known competing financial interests or personal relationships that could have appeared to influence the work reported in this paper.

CRediT authorship contribution statement

Yue Yu: Writing - original draft, Investigation, Formal analysis. **Ruiyang Zhao:** Methodology, Formal analysis. **Haichao Liu:** Writing -

review & editing, Supervision, Data curation. **Shitong Zhang:** Software, Resources. **Changjiang Zhou:** Validation. **Yu Gao:** Resources. **Weijun Li:** Conceptualization, Funding acquisition, Project administration. **Bing Yang:** Writing - review & editing.

Acknowledgements

We are grateful for supports from the National Science Foundation of China (51603185, 51673174), and Zhejiang Provincial Natural Science Foundation of China (LY19E030006, LQ19E030016, and LZ17E030001).

References

- [1] Tang CW, VanSlyke SA. Appl Phys Lett 1987;51:913–5.
- [2] Ma Y, Zhang H, Shen J, Che C. Electroluminescence from triplet metal-ligand charge-transfer excited state of transition metal complexes. Synth Met 1998;94: 245–8.
- [3] Ma C, Zhang B, Liang Z, Xie P, Wang X, Zhang B, et al. A novel n-type red luminescent material for organic light-emitting diodes. J Mater Chem 2002;12: 1671–5.
- [4] Yao YS, Xiao J, Wang XS, Deng ZB, Zhang BW. Starburst DCM-type red-light-emitting materials for electroluminescence applications. Adv Funct Mater 2006;16: 709–18.
- [5] Su SJ, Gonmori E, Sasabe H, Kido J. Highly efficient organic blue-and white-light-emitting devices having a carrier- and exciton-confining structure for reduced efficiency roll-off. Adv Mater 2008;20:4189–94.
- [6] Hsu FM, Chien CH, Shu CF, Lai CH, Hsieh CC, Wang KW, et al. A bipolar host material containing triphenylamine and diphenylphosphoryl-substituted fluorene units for highly efficient blue electrophosphorescence. Adv Funct Mater 2009;19: 2834–43.
- [7] Tao Y, Wang Q, Yang C, Zhong C, Zhang K, Qin J, et al. Tuning the optoelectronic properties of carbazole/oxadiazole hybrids through linkage modes: hosts for highly efficient green electrophosphorescence. Adv Funct Mater 2010;20:304–11.
- [8] Jeon SO, Jang SE, Son HS, Lee JY. External quantum efficiency above 20% in deep blue phosphorescent organic light-emitting diodes. Adv Mater 2011;23:1436–41.
- [9] Furue R, Matsuo K, Ashikari Y, Ooka H, Amanokura N, Yasuda T. Highly efficient red-orange delayed fluorescence emitters based on strong π -accepting dibenzophenazine and dibenzoquinoline cores: toward a rational pure-red OLED design. Adv Opt Mater 2018;6:1701147–55.
- [10] Lo YC, Yeh TH, Wang CK, Peng BJ, Hsieh JL, Lee CC, et al. High efficiency red and NIR OLED enabled by pure organic fluorescent emitters and exciplex-forming cohost. ACS Appl Mater Interfaces 2019;11:23417–27.
- [11] Ran Q, Zhang YL, Hua X, Fung MK, Liao LS, Fan J. Modulation of p-type units in tripodal bipolar hosts towards highly efficient red phosphorescent OLEDs. Dyes Pigments 2019;162:632–9.
- [12] Fleetham T, Ecton J, Li G, Li J. Improved out-coupling efficiency from a green microcavity OLED with a narrow band emission source. Org Electron 2016;37: 141–7.
- [13] Seino Y, Inomata S, Sasabe H, Pu YJ, Kido J. High-performance green OLEDs using thermally activated delayed fluorescence with a power efficiency of over 100 lm W^{-1} . Adv Mater 2016;28:2638–43.
- [14] Huang B, Ban XX, Sun KY, Ma ZM, Mei YN, Jiang M, et al. Thermally activated delayed fluorescence materials based on benzophenone derivative as emitter for efficient solution-processed non-doped green OLED. Dyes Pigments 2016;133: 380–6.
- [15] Chavez III R, Cai M, Tlach B, Wheeler DL, Kaudal R, Tsyrenova A, et al. Benzobisoxazole cruciforms: a tunable, cross-conjugated platform for the generation of deep blue OLED materials. J Mater Chem C 2016;4:3765–73.
- [16] Cui LS, Nomura H, Geng Y, Kim JU, Nakanotani H, Adachi C. Controlling singlet-triplet energy splitting for deep-blue thermally activated delayed fluorescence emitters. Angew Chem Int Ed 2017;56:1571–5.
- [17] Chan CY, Cui LS, Kim JU, Nakanotani H, Adachi C. Rational molecular design for deep-blue thermally activated delayed fluorescence emitters. Adv Funct 2018;28: 1706023–9.
- [18] Sun W, Zhou N, Xiao Y, Wang S, Li X. Novel carbazolyl-substituted spiro [acridine-9, 9'-fluorene] derivatives as deep-blue emitting materials for OLED applications. Dyes Pigments 2018;154:30–7.
- [19] Li W, Yao L, Liu HC, Wang ZM, Zhang ST, Xiao R, et al. Highly efficient deep-blue OLED with an extraordinarily narrow FWHM of 35 nm and a y-coordinate <0.05 based on a fully twisting donor-acceptor molecule. J Mater Chem C 2014;2: 4733–6.
- [20] Wang Z, Lu P, Chen S, Gao Z, Shen F, Zhang W, et al. Phenanthro [9, 10-*d*] imidazole as a new building block for blue light emitting materials. J Mater Chem 2011;21:5451–6.
- [21] Li W, Liu D, Shen F, Ma D, Wang Z, Feng T, et al. A twisting donor-acceptor molecule with an intercrossed excited state for highly efficient, deep-blue electroluminescence. Adv Funct Mater 2012;22:2797–803.
- [22] Zhang ST, Yao L, Peng Q, Li W, Pan Y, Xiao R, et al. Achieving a significantly increased efficiency in nondoped pure blue fluorescent OLED: a quasi-equivalent hybridized excited state. Adv Funct Mater 2015;25:1755–62.

- [23] Shi JJ, Xu L, Chen C, Lv XH, Ding Q, Li ZW, et al. Efficient and color-purity blue electroluminescence by manipulating the coupling forms of D-A hybrids with phenothiazine as the strong donor. *Dyes Pigments* 2019;160:962–70.
- [24] Xue SF, Qiu X, Ying SA, Lu YS, Pan YY, Sun Qk, et al. Highly efficient nondoped near-ultraviolet electroluminescence with an external quantum efficiency greater than 6.5% based on a carbazole–triazole hybrid molecule with high and balanced charge mobility. *Adv Optical Mater* 2017;5:1700747–54.
- [25] Shi JJ, Ding Q, Xu L, Lv XH, Liu ZW, Sun QK, et al. A simple D- π -A hybrid mode for highly efficient non-doped true blue OLEDs with CIEy o 0.05 and EQE up to 6%. *J Mater Chem C* 2018;6:11063–70.
- [26] Bai YQ, Hong L, Lei T, Zhang L, Ouyang XH, Liu ZY, et al. Solution-processable, single-layer, blue organic light-emitting diodes employing dual emitting cores of hybridized local and charge-transfer units. *Dyes Pigments* 2016;132:94–102.
- [27] Tang XH, Li XL, Liu HC, Gao Y, Shen Y, Zhang ST, et al. Efficient near-infrared emission based on donor-acceptor molecular architecture: the role of ancillary acceptor of cyanophenyl. *Dyes Pigments* 2018;149:430–6.
- [28] Zhou CJ, Zhang TK, Zhang ST, Liu HC, Gao Y, Su Q, et al. Isomerization effect of triphenylamine-acridine derivatives on excited-state modification, photophysical property and electroluminescence performance. *Dyes Pigments* 2017;146:558–66.